Journal of Power Sources 196 (2011) 9737–9742

Contents lists available at ScienceDirect

Journal of Power Sources

journal homepage: www.elsevier.com/locate/jpowsour

Crystal structure and physical properties of lithium difluoro(oxalato)borate (LiDFOB or $LiBF_2Ox$)

Joshua L. Allen[a], Sang-Don Han[a], Paul D. Boyle[b], Wesley A. Henderson[a,*]

[a] Ionic Liquids & Electrolytes for Energy Technologies (ILEET) Laboratory, Dept. of Chemical and Biomolecular Engineering, NC State University, 911 Partners Way, Raleigh, NC 27695-7905, USA
[b] X-ray Structural Facility, Dept. of Chemistry, NC State University, Raleigh, NC, USA

ARTICLE INFO

Article history:
Received 25 May 2011
Received in revised form 18 July 2011
Accepted 19 July 2011
Available online 26 July 2011

Keywords:
Lithium-ion battery
LiDFOB
Lithium salt
Electrolyte
Crystal structure

ABSTRACT

The structural characterization and properties of lithium difluoro(oxalato)borate (LiDFOB) are reported. LiDFOB was synthesized as previously described in the literature via direct reaction of boron trifluoride diethyl etherate with lithium oxalate. The crystal structure of the salt was determined from single crystal X-ray diffraction yielding a highly symmetric orthorhombic structure (*Cmcm*, $a = 6.2623(8)$ Å, $b = 11.4366(14)$ Å, $c = 6.3002(7)$ Å, $V = 451.22(9)$ Å^3, $Z = 4$ at 110 K). Single crystal X-ray diffraction of a dihydrate of LiDFOB yielded a monoclinic structure ($P2_1/c$, $a = 9.5580(3)$ Å, $b = 12.7162(4)$ Å, $c = 5.4387(2)$ Å, $V = 634.63(4)$ Å^3, $Z = 4$ at 110 K). Along with the crystal structures, additional structural information and the properties of LiDFOB (via ^{11}B and ^{19}F NMR, DSC, TGA and Raman spectroscopy) have been compared with those of $LiBF_4$ and LiBOB to better understand the differences between these lithium battery electrolyte salts.

1. Introduction

From the initial Li-ion technology demonstrated in the 1970s, there has been a steady improvement in electrode materials, in part to meet the demands for hybrid and electric vehicles [1]. Since commercialization of the first Li-ion battery by Sony Corp. in 1991, however, electrolyte compositions (i.e., $LiPF_6$-carbonate mixtures) have remained largely unchanged [2,3]. $LiPF_6$ has been the dominate lithium source in most electrolyte compositions for two decades, due largely to its high conductivity in carbonate-based solvents (~10 mS cm^{-1} at room temperature) and its ability to limit the corrosion of Al current collectors [4–7]. Unfortunately, $LiPF_6$ is known to decompose at elevated temperatures, resulting in the formation of LiF and PF_5, which has been shown to accelerate in the presence of carbonate-based solvents [8–10].

For Li-ion batteries to be used as a power source for electric vehicles, significant improvements must be made to current state-of-the-art electrolyte formulations to moderate the continuous capacity fade seen with current electrodes, which limits the lifetime of existing batteries. Many new lithium salts have been proposed as replacements for $LiPF_6$, but, thus far, none of the proposed salts have been able to meet the myriad property requirements necessary for commercial Li-ion batteries. Some of the lithium salts, however, have shown significant promise as additives to (i) increase ionic conductivity, (ii) decrease electrolyte flammability and/or (iii) promote interfacial stability (improved solid-electrolyte interface (SEI) formation, reduced Al corrosion, etc.).

Of the lithium salts that have been developed in the past decade, one of the most promising to date is lithium difluoro(oxalato)borate (LiDFOB). LiDFOB has been shown to form in cells containing both $LiBF_4$ and lithium bis(oxalato)borate (LiBOB) at higher temperatures, similar to the formation of lithium tetrafluoro(oxalato)phosphate (LiF_4OP) from $LiPF_6$ and LiBOB [11–13]. LiDFOB combines the benefits of its two parent molecules, $LiBF_4$ and LiBOB [14–20]:

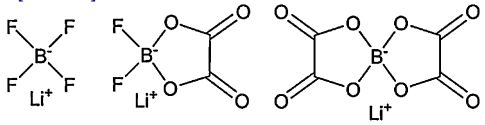

$LiBF_4$ LiDFOB LiBOB

Like LiBOB, LiDFOB has the innate ability to form a SEI on the surface of a graphite anode, even in high concentrations of propylene carbonate (PC) [17]. This intrinsic property of a lithium salt dominating SEI formation is necessary for the replacement of the high-melting ethylene carbonate (EC) that is typically required for SEI formation. LiDFOB also possesses $LiBF_4$ characteristics such as an exceptional ability to passivate the Al current collector [21].

Although LiDFOB is one of the most promising additives for battery electrolyte technologies, and numerous reports are available

* Corresponding author. Tel.: +1 919 513 2917; fax: +1 919 515 3465.
E-mail address: wesley_henderson@ncsu.edu (W.A. Henderson).

0378-7753/$ – see front matter © 2011 Elsevier B.V. All rights reserved.
doi:10.1016/j.jpowsour.2011.07.065

on its thermal/electrochemical benefits [22–36], no crystallographic data has been reported thus far. Such information provides both insight into the manner in which the anions coordinate Li^+ cations, as well as the necessary background required for computation analysis of the anion. In this study, the structural determination of LiDFOB based on single-crystal X-ray diffraction is reported. The effect of displacing fluorine atoms on BF_4^- with oxalate ligands on the thermal degradation behavior and Raman spectra has also been investigated.

2. Experimental

2.1. Materials

Anhydrous $LiBF_4$ was purchased from Sigma–Aldrich and used as-received with a purity level of 99.998% (trace metal basis). Battery-grade LiBOB was obtained gratis from Chemetall Corp.

2.2. Synthesis/purification

LiDFOB was synthesized by the direct reaction of excess boron trifluoride diethyl etherate (BF_3-ether) with lithium oxalate (oxalic acid dilithium salt), both used as-received from Sigma–Aldrich [22]. The reagents were combined in a sealed vessel and stirred for 24 h at 80 °C allowing the solid-state reaction to occur. After decanting and rinsing multiple times with ether to remove unreacted BF_3-ether, the crude lithium salt was extracted with dimethyl carbonate (DMC) and filtered to remove solid impurities (LiF, lithium oxalate, etc.). The crude lithium salt, dissolved in DMC, was roto-evaporated until small crystals formed, at which time the solution was removed, placed in a N_2 glovebox (<0.5 ppm O_2 and H_2O) and allowed to crystallize for >48 h. After decanting, the isolated crystals were then recrystallized a total of 5 times in DMC by supersaturating the solution, vacuum filtering and allowing the solution to slowly cool to promote large crystal growth. After the 5th recrystallization, LiDFOB was dried at 105 °C for 48 h, yielding a high purity salt. All actions, except the initial roto-evaporation, were performed in a N_2 glovebox. The salts ($LiBF_4$, LiDFOB and LiBOB) were dissolved in DMSO-*d*6 for NMR analysis. ^{11}B NMR was performed on a Bruker AVANCE 500 MHz spectrometer externally referenced to LiBOB at 6.60 ppm. ^{19}F NMR was performed on a Varian Mercury 300 MHz spectrometer and externally referenced to $LiPF_6$ at 65.00 ppm. Fig. 1 displays the ^{11}B- and ^{19}F NMR results, respectively, for the three salts. ^1H NMR was also performed. The NMR analysis yielded no detectable impurities.

2.3. Thermal measurements

DSC analysis was performed on a TA Instruments Q2000 differential scanning calorimeter by cooling each salt to −150 °C and heating (5 °C min^{-1}) to the salt's decomposition temperature. The instrument was calibrated with cyclohexane (solid–solid phase transition at −87.06 °C, melt transition at 6.54 °C) and indium (melt transition at 156.60 °C). The anhydrous salts were hermetically sealed in aluminium pans in the glovebox. TGA measurements were performed on a TA Instruments Q5000 thermogravimetric analyzer by heating from ambient temperature to 100 °C for 5 min to remove residual moisture from loading the sample in the instrument, cooling to RT, then heating to 600 °C at a rate of 5 °C min^{-1}. The TGA furnace was purged with N_2 gas during the measurements. DSC and TGA measurements were performed in duplicate to ensure reproducibility.

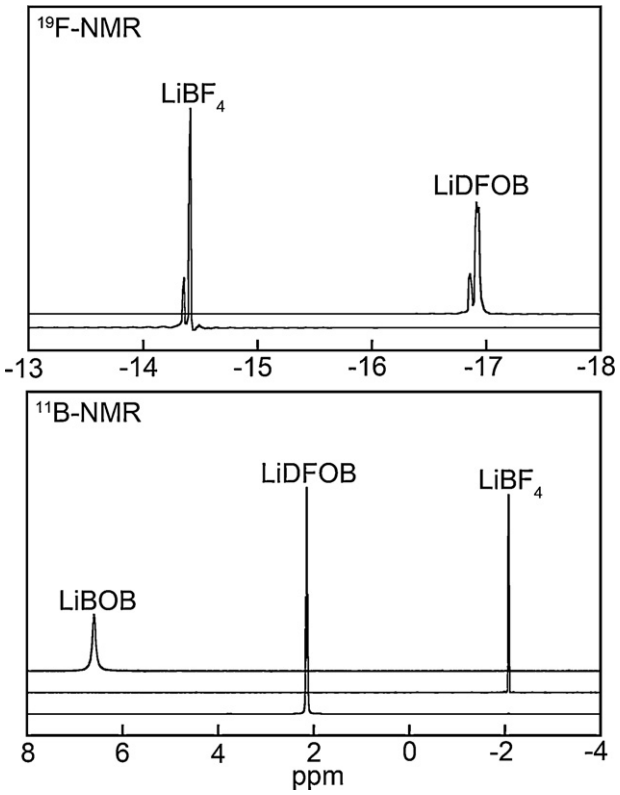

Fig. 1. ^{19}F and ^{11}B NMR spectra of LiBOB, LiDFOB and $LiBF_4$ (in DMSO-*d*6) externally referenced to $LiPF_6$ at 65.00 ppm (not shown) and LiBOB at 6.60 ppm, respectively.

2.4. Raman spectroscopy

Raman analysis was performed on a Horiba-Jobin Yvon LabRAM HR VIS confocal microscope using a 632 nm^{-1} laser as an excitation source and a Linkam stage for temperature control and protection from ambient moisture.

2.5. X-ray structural determination

LiDFOB: Single crystals were obtained from a highly concentrated solution of crude LiDFOB and DMC stored at 5 °C for approximately 30 days. A crystal was mounted on a quartz fiber with a small amount of Paratone N oil. All X-ray measurements were acquired on a Bruker-Nonius Kappa Axis X8 Apex2 diffractometer at a temperature of −163 °C [37]. The unit cell dimensions were determined from a symmetry constrained fit of 6704 reflections with $7.42^\circ < 2\theta < 81.78^\circ$. The data collection strategy was a number of ω and φ scans which collected data up to 84.8° (2θ).

LiDFOB·2H$_2$O: Single crystals were obtained from a solution of DMC and LiDFOB that was exposed to ambient moisture. A single crystal was mounted on a Mitegen polyimide micromount with a small amount of Paratone N oil. All X-ray measurements were made on a Bruker-Nonius Kappa Axis X8 Apex2 diffractometer at a temperature of −163 °C [37]. The unit cell dimensions were determined from a symmetry constrained fit of 9916 reflections with $5.48^\circ < 2\theta < 83.72^\circ$. The data collection strategy was a number of ω scans which collected data up to 85.56° (2θ).

Refinement: The frame integration was performed using SAINT [37]. The resulting raw data was scaled and absorption corrected using a multi-scan averaging of symmetry equivalent data using SADABS [37]. Details of the crystal structure data can be found in Table 1 and the Supplemental Data. The structures were solved by direct methods using the XS program from SHELXS [38]. All non-hydrogen atoms were obtained from the initial solution. The

Table 1
Crystal data and structural refinement for LiDFOB and its dihydrate.

	LiDFOB	LiDFOB·$2H_2O$
Empirical formula	$C_2BF_2LiO_4$	$C_2H_4BF_2LiO_6$
Formula weight	143.77	179.80
Temperature	110 K	
Wavelength	0.71073 Å	
Crystal system	Orthorhombic	Monoclinic
Space group	*Cmcm*	$P2_1/c$
a (Å)	6.2623(8)	9.5580(3)
b (Å)	11.4366(14)	12.7162(4)
c (Å)	6.3002(7)	5.4387(2)
V (Å^3)	451.22(9)	634.63(4)
Z	4	4
D_{calc} (g cm^{-3})	2.116	1.882
Abs. coeff. (mm^{-1})	0.235	0.209
F(0 0 0)	280	360
Index ranges	$-11 \le h \le 11$	$-18 \le h \le 16$
	$0 \le k \le 20$	$-22 \le k \le 23$
	$0 \le l \le 12$	$-8 \le l \le 9$
θ range (°)	$3.71 \le \theta \le 40.89$	$2.74 \le \theta \le 41.86$
Reflections collected	15,751	37,576
Reflections unique	857	4060
Reflections observed	731	3227
Refinement method	Full-matrix least-squares on F^2	
Data/restraints/parameters	857/0/33	4060/0/125
Goof	1.126	1.008
Final *R* indices [$I > 2\sigma(I)$]	$R1 = 0.0330$	$R1 = 0.0297$
	w$R2 = 0.0838$	w$R2 = 0.0745$
R indices (all data)	$R1 = 0.0414$	$R1 = 0.0430$
	w$R2 = 0.0876$	w$R2 = 0.0815$
$\Delta e_{min}/\Delta e_{max}$ (e Å^{-3})	−0.363/0.641	−0.326/0.478

hydrogen atom positions were obtained from a difference Fourier map and were allowed to refine isotropically. The structural model was fit to the data using full matrix least-squares based on F^2. The calculated structure factors included corrections for anomalous dispersion from the usual tabulation. The structures were refined using the XL program from SHELXTL [38].

3. Results and discussion

3.1. Crystal structure of LiDFOB and LiDFOB·$2H_2O$

LiDFOB: The single crystal structure of LiDFOB is a highly symmetric, orthorhombic structure with lattice parameters $a = 6.2623(8)$ Å, $b = 11.4366(14)$ Å, $c = 6.3002(7)$ Å and $\beta = 90.00°$ (space group *Cmcm*).The ion packing in LiDFOB is shown in Fig. 2. Each Li^+ cation is coordinated by 4 oxygen atoms from 3 $DFOB^-$ anions and 2 fluorine atoms from 2 $DFOB^-$ anions with some similarities to both $LiBF_4$ and LiBOB [39,40]. Each $DFOB^-$ anion is coordinated to 5 Li^+ cations. The anion oxalate group coordinates 3 of the cations through the carbonyl oxygens with one cation coordinated by both carbonyl groups. Each fluorine atom is coordinated to a single Li^+ cation. This coordination results in the $DFOB^-$ anions and Li^+ cations being arranged in planar sheets which are linked together by the fluorine–Li^+ cation coordination bonds. A comparison of the Li^+ cation and anion coordination within the $LiBF_4$, LiDFOB and LiBOB crystal structures is displayed in Fig. 3.

LiDFOB·$2H_2O$: The single crystal structure of LiDFOB·$2H_2O$ is a monoclinic structure with lattice parameters $a = 9.5580(3)$ Å, $b = 12.7162(4)$ Å, $c = 5.4387(2)$ Å and $\beta = 106.2469(12)°$ (space group $P2_1/c$). The ion packing in LiDFOB·$2H_2O$ can be seen in Fig. 2. Each Li^+ cation is coordinated by 2 oxygen atoms from 2 $DFOB^-$ anions and 4 oxygen atoms from 4 H_2O molecules. Each H_2O molecule is coordinated to 2 Li^+ cations and the oxalate group from each $DFOB^-$ anion coordinates 2 Li^+ cations through a single carbonyl oxygen. This coordination results in polymeric chains in which the fluorine atoms from the $DFOB^-$ anions and hydrogens from H_2O are protruding out of the unit cell (Fig. 2).

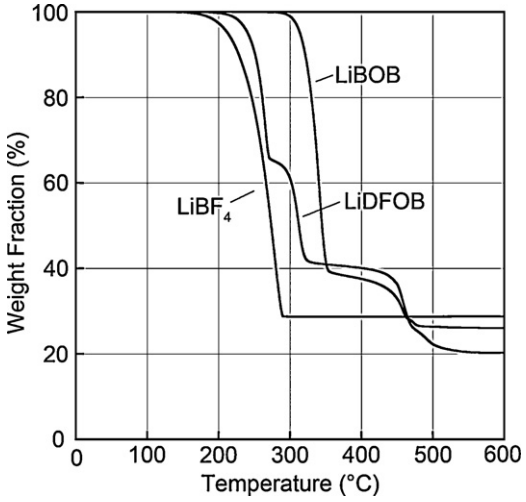

Fig. 5. TGA heating traces (5 °C min^{-1}) of $LiBF_4$, LiDFOB and LiBOB.

3.2. Thermal properties of LiDFOB

The thermal properties of each lithium salt differ significantly in the DSC and TGA measurements (Figs. 4 and 5). For instance, after a solid–solid phase transition at 28 °C [40], $LiBF_4$ displays an endothermic peak at 305 °C (melting and/or decomposition) (DSC). The TGA measurements, however, show that $LiBF_4$ mass loss onset occurs at ~160 °C. This behavior is also seen with LiDFOB; an endothermic peak exists at 272 °C (DSC), but mass loss onset occurs at ~200 °C (TGA). These results indicate that vapor pressure may play a significant role in the thermal degradation of each lithium salt as the TGA measurement involves heating the sample open to flowing N_2 gas, whereas for the DSC measurements the Al sample pans are hermetically sealed in the N_2-filled glove box. These measurements are reproducible.

TGA is useful for determining the lithium salt's decomposition products, which can aid in the identification of impurities that may exist within an electrolyte, as well as battery thermal runaway processes. The thermal decomposition mechanism of $LiBF_4$ is known (Reaction 1) [42] and can be easily related to its TGA thermogram (Fig. 5). The loss of BF_3 correlates with a 72.3% reduction in mass, which is observed in the TGA as a single-step decomposition:

$$LiBF_4 \rightarrow LiF_{(s)} + BF_{3(g)} \quad (1)$$

The thermal decomposition of LiBOB is much more intricate. Zinigrad et al. report a multi-step thermal decomposition of LiBOB (<350 °C), which can be related to the mass loss seen in the TGA measurements (reactions 2 and 3). The initial decomposition step at ~350 °C (DSC) or 290 °C (TGA) is a combination of reactions (2) and (3), as reported in the literature [18]. These reactions account for a 61.9% reduction of mass:

$$6LiBC_4O_8 \rightarrow 3Li_2C_2O_{4(s)} + 3B_2O_{3(s)} + 9CO_{(g)} + 9CO_{2(g)} \quad (2)$$

$$Li_2C_2O_4 + 3B_2O_3 \rightarrow 2LiB_3O_{5(s)} + CO_{(g)} + CO_{2(g)} \quad (3)$$

The final LiBOB decomposition step may involve the decomposition of the remaining lithium oxalate due to its reported decomposition temperature of ~520 °C [43]. This decomposition step, however, has not been further investigated and has thus far not been reported in the literature.

It appears from the TGA analysis that LiDFOB may be a combination of the two decomposition mechanisms for both $LiBF_4$ and

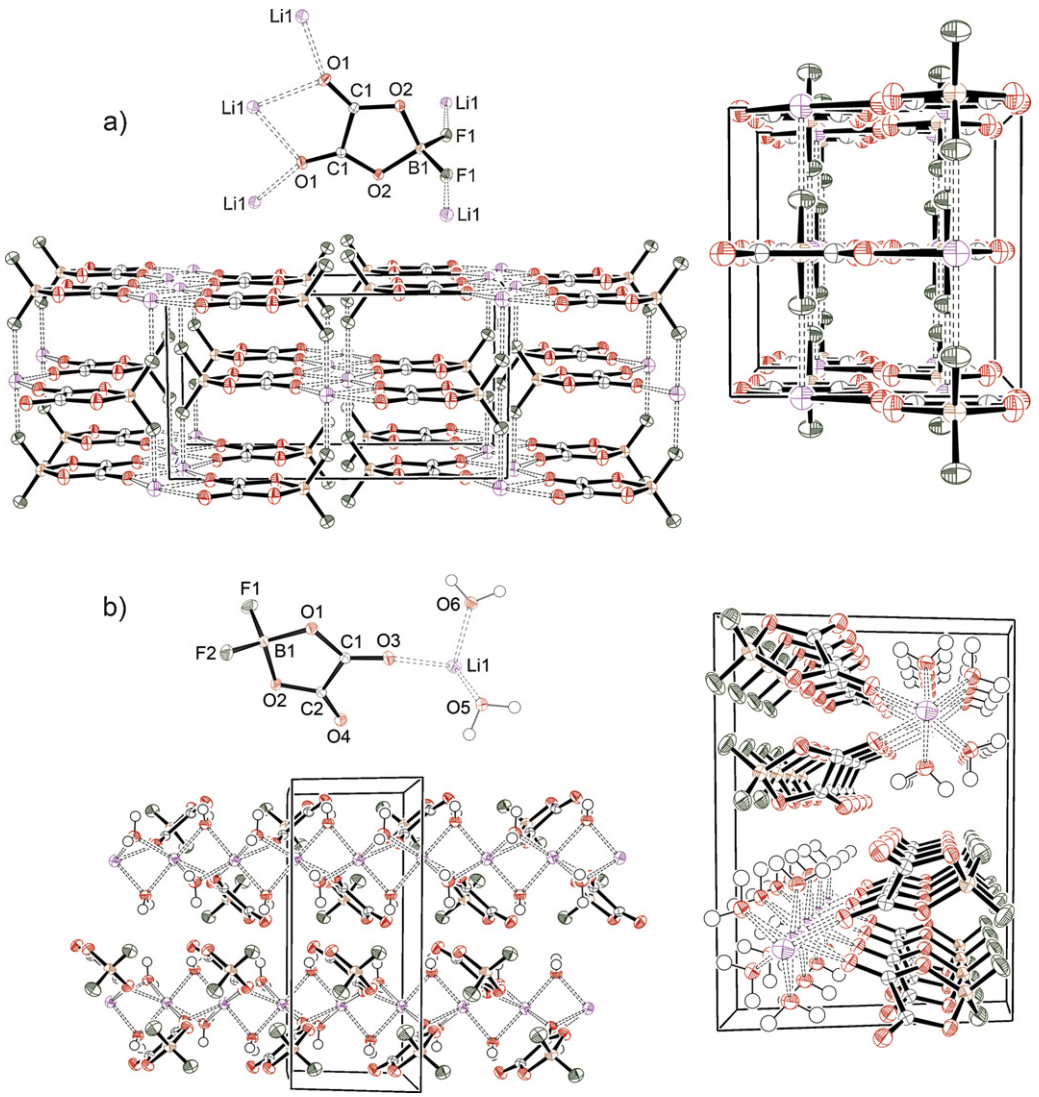

Fig. 2. Ion packing in the crystal structures of (a) LiDFOB and (b) LiDFOB·$2H_2O$.

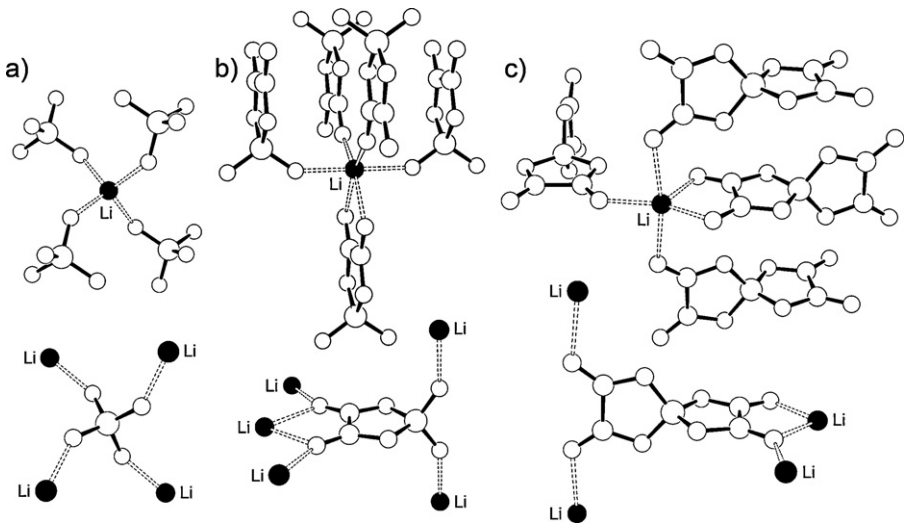

Fig. 3. Li^+ cation (top) and anion (bottom) coordination in the crystal structures of (a) $LiBF_4$ [40], (b) LiDFOB and (c) LiBOB [41].

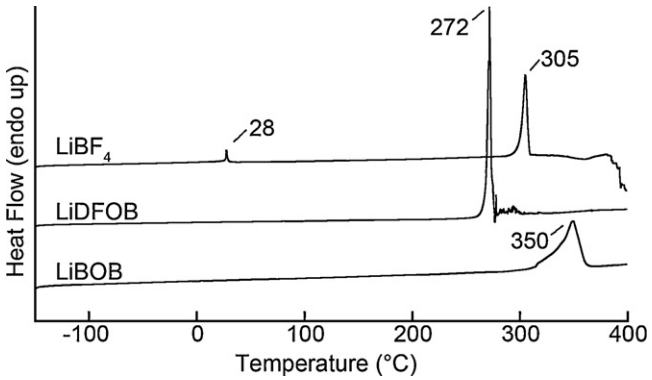

Fig. 4. DSC heating traces (5 °C min^{-1}) of $LiBF_4$, LiDFOB and LiBOB.

LiBOB. However, attempts to interpret the decomposition products have thus far been unsuccessful. It is believed that similar products will be formed, but the exact stoichiometric ratios remain unknown.

3.3. Raman spectra

The highest intensity peak in the $LiBF_4$ Raman spectra is from a symmetric B–F stretching mode, which has a characteristic peak in the 760–800 cm^{-1} region [44]. This peak is known to shift due to varying forms of ionic association between the anion and cations [44,45]. The B–F stretching peak of the neat lithium salt can be seen in Fig. 6 at 797 cm^{-1}.

LiBOB has been studied via vibrational spectroscopy (IR and Raman) and *ab initio* calculations [46,47]. By comparing the peak assignments of LiBOB to LiDFOB, a preliminary interpretation for the Raman spectra of LiDFOB can be provided. Holomb et al. report that the BOB^- anion displays out-of-phase valence vibrations at ~1780 cm^{-1} and ~1800 cm^{-1}, as well as an in-phase valence vibration at 1822 cm^{-1}, corresponding to C=O vibrations [47]. Since $DFOB^-$ also possesses these C=O bonds, it is reasonable to assume that the peaks at 1762 cm^{-1} and 1800 cm^{-1} correspond to out-of-phase and in-phase valence vibrations, respectfully. These peaks shift and/or split from Li^+ cation coordination effects that are present in the neat lithium salt and solvates in solution [46].

Other peak assignments can be analyzed based upon the similarity in structure of the $DFOB^-$ and BOB^- anions, including a (O=C–C=O) bend at 360 cm^{-1}, (O–B–O) deformation at 722 cm^{-1}, (O–B–O) valence and (O–C–O) deformation at 946 cm^{-1}, and (C–O) valence (in-phase) and (C–C) valence at 1405 cm^{-1} [47]. When a single Li^+ cation is coordinated by the two oxalate carbonyl oxygens, the C–C stretching vibration calculated to be 1328 cm^{-1} (for uncoordinated BOB^-) shifts to ~1435 cm^{-1} due to the formation of a contact ion-pair [47]. In contrast, the crystal structure of LiDFOB has carbonyl oxygens coordinated to three Li^+ cations, one of which is coordinated by both carbonyl groups (Fig. 3). This coordination within the LiDFOB crystal structure may result in the single Raman peak at 1404 cm^1 (Fig. 6). In LiBOB, multiple peaks are present in the 1300–1450 cm^{-1} range. These peaks likely result from the coordination of the anion to multiple Li^+ cations in various ways (Fig. 3), causing distinct C–C stretching bands to form as a function of the type of cation coordination. *Ab initio* calculations have suggested that the best peak for analyzing the ionic association interactions (i.e., Li^+ cation coordination) may be the shift of the Raman C–C stretching vibration peak from ~1330 cm^{-1} (for the uncoordinated anion) to ~1400 cm^{-1} (for the anion coordinated through the oxalate group) [47].

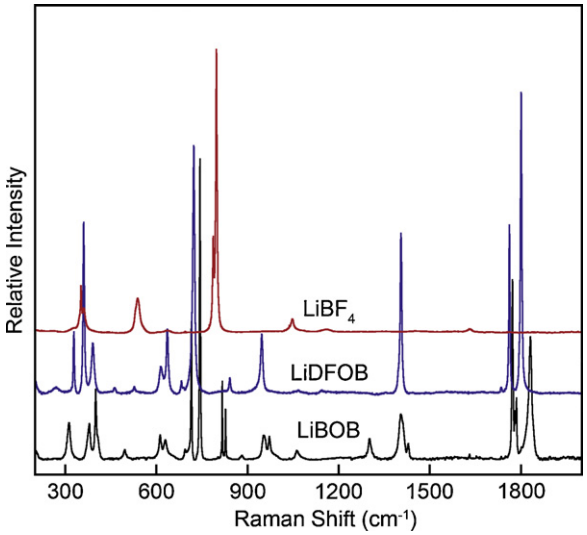

Fig. 6. Raman spectra of $LiBF_4$, LiDFOB and LiBOB.

4. Conclusions

The structural determination of the crystal structure of LiDFOB has shown that the Li^+ cations are coordinated by both fluorine and oxygen atoms. The $DFOB^-$ anions are coordinated to 5 Li^+ cations with the anion's oxalate group coordinated to 3 cations through the carbonyl oxygen atoms, with one of the Li^+ cations coordinated by both carbonyl oxygen atoms. Each anion fluorine atom is coordinated to a single Li^+ cation. In contrast, in $LiDFOB{\cdot}2H_2O$, the Li^+ cations are coordinated by a total of 6 oxygen atoms. The H_2O molecules are coordinated to 2 Li^+ cations. Each Li^+ cation is coordinated by 2 $DFOB^-$ anions through their carbonyl oxygen atoms and 4 H_2O molecules. Each $DFOB^-$ anion is coordinated to 2 Li^+ cations, resulting in ionic polymeric chains. The thermal decomposition of LiDFOB displays similarities to both $LiBF_4$ and LiBOB. Although the decomposition products of both $LiBF_4$ and LiBOB are well studied, and it appears that LiDFOB decomposition is a combination of these pathways, the actual decomposition products of LiDFOB are yet to be determined. Based upon the DSC and TGA analysis of all three salts, vapor pressure appears to play a significant role in the thermal decomposition, leading to a much higher thermal stability in a sealed system. The similarities of $DFOB^-$ and BOB^- coordination to Li^+ cations results in similar Raman spectra for the two Li^+ salts. Thus, calculated vibrational band assignments for the BOB^- anion have been used to interpret the $DFOB^-$ anion peak assignments.

Supplementary data

Crystallographic data tables (PDF) for LiDFOB and $LiDFOB{\cdot}2H_2O$ are available free of charge via the internet at http://www.elsevier.com. Crystallographic information files (cifs) for the reported structures can be obtained free of charge from The Cambridge Crystallographic Data Centre (CCDC) via the internet at www.ccdc.cam.ac.uk/data_request/cif (deposition numbers 824300 and 824301).

Acknowledgements

This work was fully funded by the U.S. DOE BATT Program (contract number DE-AC02-05-CH11231). J.L.A. would like to thank the SMART Scholarship Program and the American Society for Engineering Education (ASEE) for the award of a SMART Graduate Research Fellowship.

Appendix A. Supplementary data

Supplementary data associated with this article can be found, in the online version, at doi:10.1016/j.jpowsour.2011.07.065.

References

[1] M.S. Whittingham, Science 192 (1976) 1126.
[2] K. Ozawa, Solid State Ionics 69 (1994) 212.
[3] K. Xu, Chem. Rev 104 (2004) 4303.
[4] M.S. Ding, K. Xu, S.S. Zhang, K. Amine, G.L. Henriksen, T.R. Jow, J. Electrochem. Soc. 148 (2001) A1196.
[5] M. Ding, R. Jow, J. Electrochem. Soc. 150 (2003) A620.
[6] H. Yang, K. Kwon, T. Devine, J. Evans, J. Electrochem. Soc. 147 (2000) 4399.
[7] S. Zhang, R. Jow, J. Electrochem. Soc. 109 (2002) 458.
[8] S.E. Sloop, J.K. Pugh, S. Wang, J.B. Kerr, K. Kinoshita, Electrochem. Solid-State Lett. 4 (2001) A42.
[9] T. Kawamura, S. Okada, J. Yamaki, J. Power Sources 156 (2006) 547.
[10] E. Zinigrad, L. Larush-Asraf, J. Gnanaraj, M. Sprecher, D. Aurbach, Thermochim. Acta 438 (2005) 184.
[11] A. Xiao, L. Yang, B. Lucht, J. Electrochem. Soc. 10 (2007) A241.
[12] M. Xu, A. Xiao, L. Weishan, B. Lucht, Electrochem. Solid-State Lett. 12 (2009) A155.
[13] Y. Qin, Z. Chen, J. Liu, K. Amine, Electrochem. Solid-State Lett. 13 (2010) A11.
[14] M. Ue, J. Electrochem. Soc. 141 (1994) 3336.
[15] S. Zhang, K. Xu, R. Jow, Electrochem. Commun. 4 (2002) 928.
[16] S. Zhang, K. Xu, R. Jow, J. Power Sources 156 (2006) 629.
[17] K. Xu, S. Zhang, B.A. Poese, R.T. Jow, Electrochem. Solid-State Lett. 5 (2002) A259.
[18] E. Zinigrad, L. Larush-Asraf, G. Salitra, M. Sprecher, D. Aurbach, Thermochim. Acta 457 (2007) 64.
[19] S. Li, P. Ma, S. Song, Q. Ren, F. Li, Russ. J. Electrochem. 44 (2008) 1144.
[20] M. Ding, K. Xu, R. Jow, J. Electrochem. Soc. 152 (2005) A132.
[21] S.S. Zhang, Electrochem. Commun. 8 (2006) 1423.
[22] S.S. Zhang, J. Power Sources 163 (2007) 713.
[23] Z. Chen, Y. Qin, J. Liu, K. Amine, Electrochem. Solid-State Lett. 12 (2009) A69.
[24] Z. Chen, J. Liu, K. Amine, Electrochem. Solid-State Lett. 12 (2007) A45.
[25] M.H. Fu, K.L. Huang, S.Q. Liu, J.S. Liu, Y.K. Li, J. Power Sources 195 (2010) 862.
[26] S.S. Zhang, ECS Trans. 3 (2007) 59.
[27] E. Zygadlo-Monikowska, Z. Florjanczyk, P. Kubisa, T. Biedron, A. Tomaszewska, J. Ostrowska, N. Langwald, J. Power Sources 195 (2010) 6202.
[28] H.-Q. Gao, Z.-A. Zhang, Y.-Q. Lai, J. Li, Y.-X. Liu, J. Cent. South. Univ. Technol. 15 (2008) 830.
[29] J. Hunag, L.-Z. Fan, B. Yu, T. Xing, W. Qiu, Ionics 16 (2010) 509.
[30] Z. Zhang, X. Chen, F. Li, Y. Lai, J. Li, P. Liu, X.J. Wang, J. Power Sources 195 (2010) 7397.
[31] S. Li, X. Xu, X. Shi, X. Cui, Adv. Mater. Res. 197–198 (2011) 1121.
[32] J. Liu, Z. Chen, S. Busking, K. Amine, Electrochem. Commun. 9 (2007) 475.
[33] S.-H. Kang, D.P. Abraham, A. Xiao, B.L. Lucht, J. Power Sources 175 (2008) 526.
[34] J. Liu, Z. Chen, S. Busking, I. Belharouak, K. Amine, J. Power Sources 174 (2007) 852.
[35] M. Xu, L. Zhou, L. Hao, L. Xing, W. Li, B.L. Lucht, J. Power Sources (2010), doi:10.1016/j.jpowsour.2010.10.050.
[36] A. Lex-Balducci, R. Schmitz, R.W. Schmitz, R. Muller, M. Amereller, D. Moosbauer, H. Gores, M. Winter, ECS Trans. 25 (2010) 13.
[37] Apex2, SAINT and SADABS, Bruker ASX Inc., Madison, Wisconsin, USA, 2009.
[38] G.M. Sheldrick, Acta Crystallogr. A64 (2008) 112.
[39] K. Matsumoto, R. Hagiwara, Z. Mazej, E. Goreshnik, B. Zemva, J. Phys. Chem. A 110 (2006) 2138.
[40] P. Zavalij, S. Yang, S. Whittingham, Acta Crystallogr. B59 (2003) 753.
[41] G. Sharpataya, K. Gavrichev, V. Platkhotnik, Zh. Neorg. Khim. 42 (1997) 649.
[42] A. Kana'an, J. Kanamueller, High Temp. Sci. 11 (1979) 23.
[43] D. Dollimore, D. Tinsley, J. Chem. Soc. A 19 (1971) 3043.
[44] X. Xuan, H. Zhang, J. Wang, H. Wang, J. Phys. Chem. A 108 (2004) 7513.
[45] H. Qiao, H. Luan, Z. Zhou, L. Bi, W. Yao, J. Li, C. Chen, J. Mol. Struct. 885 (2008) 89.
[46] Z. Yu, T. Xu, T. Xing, L.-Z. Fan, F. Lian, W. Qiu, J. Power Sources 196 (2010) 4285.
[47] R. Holomb, W. Xu, H. Markusson, P. Johansson, P. Jacobsson, J. Phys. Chem. A 110 (2006) 11467.